Nanostructures

Metastable Vanadium Dioxide Nanobelts: Hydrothermal Synthesis, Electrical Transport, and Magnetic Properties**

*Junfeng Liu, Qiuhong Li, Taihong Wang, Dapeng Yu, and Yadong Li**

One-dimensional (1D) nanostructures have attracted a great deal of attention as functional units for mediating the transport of electrons or optical excitations. Probing their intrinsic properties is critical to assess their possible roles in new types of nanoscale devices.[1–3] Because of some critical limitations that are difficult to overcome in carbon nanotubes, many other 1D nanostructures have been developed.[4–16]

[*] J. Liu, Prof. Y. Li
Department of Chemistry and
the Key Laboratory of Atomic & Molecular Nanosciences
(Ministry of Education, China)
Tsinghua University
Beijing, 100084 (P.R. China)
and
National Center for Nanoscience and Nanotechnology
Beijing, 100084 (P.R. China)
Fax: (+86) 10-6278-8765
E-mail: ydli@tsinghua.edu.cn
Q. Li, Prof. T. Wang
Institute of Physics
Chinese Academy of Sciences
Beijing (P.R. China)
Prof. D. Yu
Department of Physics
Peking University
Beijing (P.R. China)

[**] This work was supported by NSFC (50372030, 20025102, 20151001), the Foundation for the Author of National Excellent Doctoral Dissertation of P.R. China, and the state key project of fundamental research in nanomaterials and nanostructures (2003CB716901).

  DOI: 10.1002/ange.200460104

VO_2(B), one of metastable phases of vanadium dioxide, is of great interest owing to its layered structure and promising properties in the nanometer regime.[17–19] It is an attractive material for various applications especially as an electrode material for lithium batteries. VO_2(B) exhibits a maximum reversible capacity of about 320 mA h g^{-1} in the range 4 to 1 V in lithium cells.[17,18] Huynh et al. reported that the operating properties of batteries depend not only on the structure, but also on the morphology of the electrode components.[20] It was shown that 1D nanostructures are more prone to charge transport than the bulk crystalline structures. VO_2(B) can be prepared by traditional methods such as thermal reduction of V_2O_5 by H_2 or SO_2 gas, thermal decomposition of ammonium hexavanadate, and reduction of aqueous vanadate solution with potassium borohydride.[21,22] However, most of the synthetic routes only lead to bulk VO_2(B), and the synthesis of VO_2(B) 1D nanostructures is still a challenge to material scientists. Herein, we report a convenient and controllable approach for the synthesis of metastable monoclinic vanadium dioxide single-crystal nanobelts, which requires neither sophisticated techniques nor catalysts. The electrical transport through individual nanobelts as well as the magnetic properties of these materials have also been investigated.

VO_2(B) consists of three-dimensional frameworks of VO_6 octahedra and adopts a structure derived from the structure of V_2O_5.[21] Recently, we have obtained V_2O_5 nanobelts by hydrothermal synthesis by treating ammonium metavanadate with nitric acid. Thus, it was anticipated that the low-valent 1D vanadium oxides could be obtained by adding an appropriate mild reducing agent under similar hydrothermal conditions. Our experiments have revealed that formic acid can function both as the acidification and reducing agent and has enabled us to prepare the metastable phase of vanadium dioxide nanobelts on a large scale.

The basic reaction we employed for the synthesis of the VO_2 nanobelts can be formulated in Equation (1), which in turn comprises two half reactions [Eq. (2) and (3)].

$$2\,VO_3^- + HCOOH + 2\,H^+ \rightarrow 2\,VO_2 + CO_2 + 2\,H_2O \quad (1)$$

$$VO_3^- + 2\,H^+ + e^- \rightarrow VO_2 + H_2O \quad E^o = +1.00\,V \quad (2)$$

$$CO_2 + 2\,H^+ + 2\,e^- \rightarrow HCOOH \quad E^o = -0.20\,V \quad (3)$$

On the basis of standard reduction potential ($E°$) values, the standard Gibbs free energy change $\Delta G_m°$ of the redox reaction [Eq. (1)] was estimated to be $-231.6\,kJ\,mol^{-1}$, implying a very strong tendency for the reaction to progress toward the products.

By controlling the pH value and the temperature, the nanobelts could be conveniently prepared without the presence of template or catalyst. It is noteworthy that the as-synthesized nanobelts can be either prepared as stable colloidal solutions or self-assemble into the "paper form" only after suction filtration. Typical X-ray diffraction (XRD) patterns of the VO_2(B) nanobelts are given in Figure 1. Figure 1a shows a set of reflections at 14.4°, 29.0°, and 44.1° for the VO_2(B) nanobelts that assembled into the paper form, characteristic of (00l) reflections for layered phases of

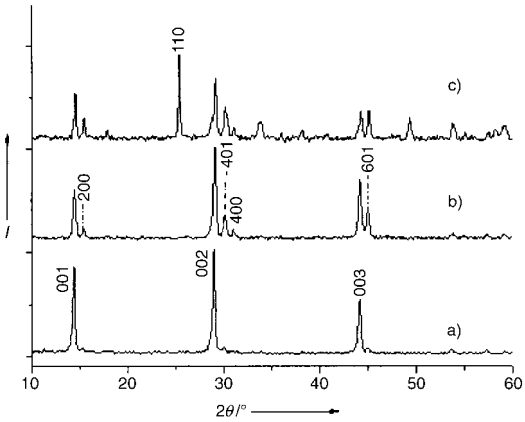

Figure 1. XRD patterns of VO_2(B). a) VO_2 film (the "paper-form" product obtained directly after filtering); b) the partly broken "paper-form" product; c) VO_2(B) powders ground from the "paper-form" product.

VO_2(B). The layer spacing of the phase is determined to be 6.15 Å from the (001) reflection. When the "paper-form" product was broken into pieces, peaks appeared in the XRD pattern at (200), (400), (−401), (−601) (Figure 1b). Finally, after the sample was thoroughly ground, all the peaks can be perfectly indexed to the monoclinic VO_2(B) phase (space group: $C2/m$) with lattice constants $a = 12.09$, $b = 3.702$, $c = 6.433$ Å, and $\beta = 106.6°$(JCPDS 81–2392) (Figure 1c). Interestingly, no peaks of any other phases or impurities were detected. In Figure 1c the more intense peaks are consistent with the JCPDS card, including the strongest peak at (110). But in the paper-form sample, most of these peaks are missing and only (00l) peaks appeared. Considering these results with regard to the crystal structure of VO_2(B), it appears that most of the nanobelts packed along (001) in the paper-form sample, and the [010] direction was the growth axis of the belts.

The size and morphology of the products were also examined by scanning electron microscopy (SEM) and transmission electron microscopy (TEM). As shown in Figure 2, the VO_2 nanobelts are several micrometers long, typically 50–100 nm wide, and 10–20 nm thick. In addition, the TEM image and the selected area electron diffraction (SAED) pattern of an individual nanobelt are shown in Figure 2c. The [010] direction of the electron diffraction pattern is parallel to the belt axis, showing that growth occurs along the [010] direction, which is in agreement with the conclusion from the XRD pattern. A high-resolution TEM (HRTEM) image provides an insight into the prepared nanobelt structure. The HRTEM image (Figure 2d) of the end of an individual VO_2 nanobelt shows that it is a single crystal without the presence of dislocations and defects. The 17° orientation between the (010) and (110) lattice planes is consistent with the crystal structure. Energy-dispersive X-ray analysis (EDAX) spectra were also measured to determine the chemical composition of the as-prepared VO_2 nanobelts. Results from EDAX spectra show that the nanobelts only contain V and O; however, the atom ratio of V and O cannot be determined because one peak for the element V overlaps with the peak for the element O.

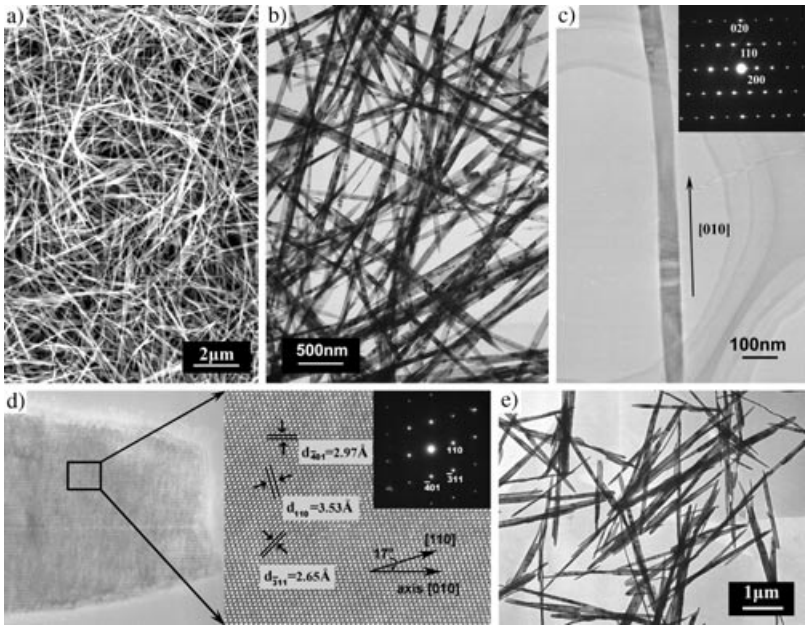

Figure 2. Typical field-emission SEM (a) and low-resolution TEM (b) images of the VO_2(B) nanobelts. c) Individual nanobelt on the [001] plane. d) HRTEM image of the end of VO_2 nanobelts showing that the nanobelt is single crystalline and free from dislocation and defects. The 17° orientation between [110] and long axis shows the growth direction to be [010]. e) VO_2(B) nanobelts synthesized in excess formic acid (pH 2).

The synthesis parameters, such as the pH value, temperature, and reaction time, play an important role in controlling the morphology. A series of experiments showed that using a lower temperature resulted in a V_2O_5 gel owing to the inefficient reduction, and shorter reaction times led to bad crystallization. Little product was generated at a pH > 3 owing to insufficient acidification, and only when the pH value was lower than 3 were large amounts of VO_2(B) nanobelts obtained. The average aspect ratio and width-to-thickness ratio of the nanobelts dropped as the pH value of the synthesis solution decreased from 3 to 2 on increasing the amount of formic acid. When the pH value was adjusted to 3, long belts were obtained for which the average aspect ratio was more than 100 and the width-to-thickness ratio was about 10 (Figure 2b). At a pH 2 the morphology of the vanadium dioxide changed from nanobelts to nanorods with a length of 2–3 μm and an aspect ratio of 20–30 (Figure 2e).

Further advancement of this approach for nanobelt synthesis requires a clear understanding of the growth mechanism. The growth axis of the nanobelt is related to its crystallographic characteristics. VO_2(B) is constructed from two different layers of VO_6 octahedra. When viewed down the *c* axis, VO_2(B) exhibits two edge-sharing octahedra to produce a layer of "steplike" octahedra. These layers are linked to each other at the protruding corners of each pair of octahedra to produce a three-dimensional framework (Figure 3).[23]

The growth direction of the VO_2 crystal may be determined by the relative stacking rate of the octahedra at various crystal faces. As for the interface of VO_2, the longest bond (V1–O3) is 2.677 Å (Figure 3), which makes [001] the slowest growth direction, and the average shortest bond along the [010] direction indicates that the (010) plane has a relatively high stacking rate, which favors growth along the [010] axis. It is believed that detailed studies on the crystal structure and the symmetry will help to explain the results, and could also provide insight into how to control the morphology.

The transport properties of single-crystalline vanadium dioxide nanobelts have been investigated in vacuum by scanning the bias voltage. The 50-nm Au electrodes were deposited by e-beam deposition on a Si substrate covered with a 500-nm thick thermally grown SiO_2 layer. Then an individual vanadium dioxide nanobelt was deposited from an ethanol solution onto the top of the electrodes. A schematic illustration of our device and a typical SEM image recorded with it are given in Figure 4a. The distance between the two electrodes was about 500 nm. The measurements were performed in a vacuum of 3×10^{-5} mbar.

At room temperature, the samples exhibited nonlinear, symmetric current/voltage (I/V) characteristics (Figure 4b). The curve is reproducible and no large fluctuations are observed even in the high bias region, indicating that the device is stable. The I–V curve shows superlinear behavior, and closely follows the empirical formula: $I = a + bV + cV^2 + dV^3$, with experimental coefficients of $a \approx 0$, $b = 1.97$, $c = -0.01$, and

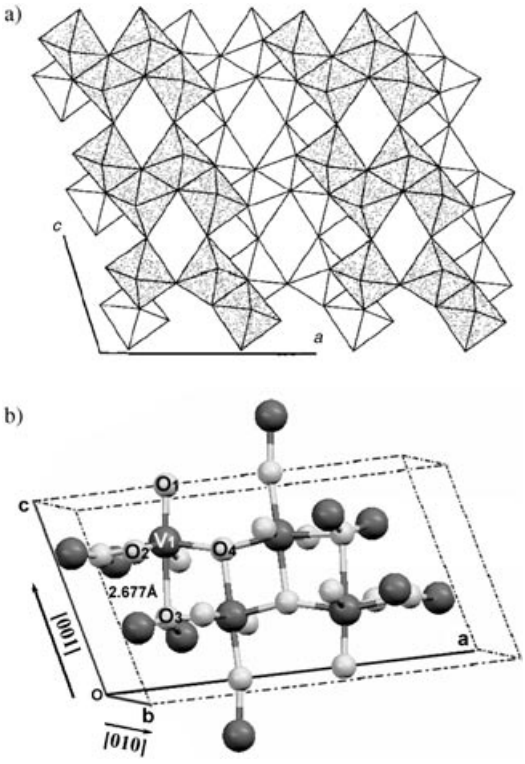

Figure 3. a) Projection of the VO_2(B) structure along [010]. b) Crystal structure of VO_2(B) nanobelts. The longest bond (V1–O3) is 2.677 Å, which makes [001] the smallest growth direction, and the average shortest bond along the [010] direction makes the (010) plane have the highest stacking rate.

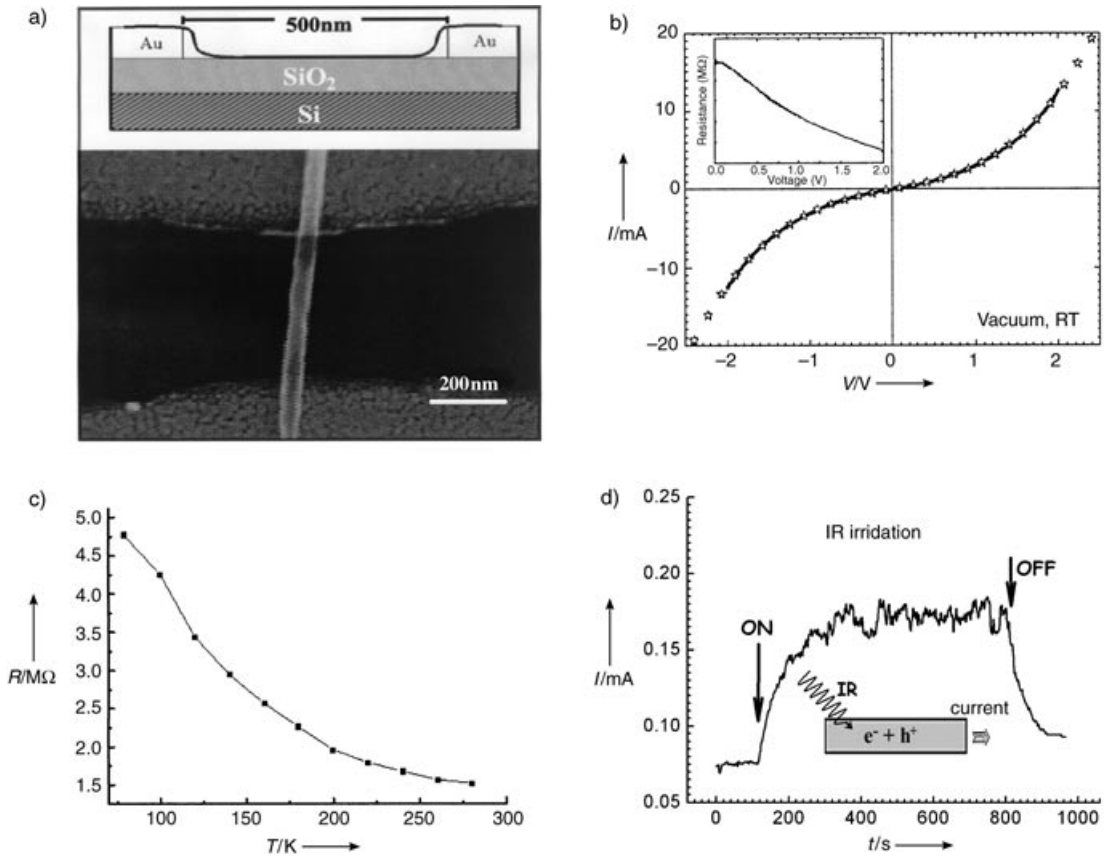

Figure 4. a) Schematic illustration of our device and a typical SEM image. b) *I*/*V* characteristics of the individual nanobelt at room temperature (solid line) and the empirical formula $I = a + bV + cV^2 + dV^3$ (starred line). The inset shows the plot of the resistance $R = V/I$ versus bias voltage *V*. c) Plot of the temperature dependence of the resistance *R*. d) IR response of a single nanobelt in vacuum. The inset is a schematic representation of the mechanism of the IR response.

$d = 1.05$. As shown in Figure 4b, the curves for the empirical formula and the current coincide with each other very well. The temperature dependence of the resistance is displayed in Figure 4c, which shows that the resistance increases as the temperature drops from 280 K to 50 K.

We analyzed the optoelectronic response of the device in vacuum. The behavior of a representative nanobelt is shown in Figure 4d. When exposed to IR light, the nanobelt conductance increased two- to threefold and stabilized within 1–2 min. The rise in conductance is due to the generation of photocurrent, which directly increases the number of free carriers within the device (inset pattern in Figure 4d). The effect was fully reversible when the light was turned off, with 90% decay of the photoresponse in 100–200 s. The photoswitching behavior was reproducible.

The magnetization of the as-prepared VO_2 nanobelts was measured with a superconducting quantum interference device (SQUID) magnetometer. The magnetization curves as a function of the applied field at 5 K under conditions of zero-field cooling (ZFC) and field cooling (FC) in a 100 Oe field are shown in Figure 5. The results indicate VO_2(B) nanobelts are paramagnetic materials.

In summary, we synthesized metastable monoclinic vanadium dioxide single-crystal nanobelts by a direct hydrothermal reduction method. The obtained nanobelts crystallize well and allow dimensional control along the [010] direction. The single-crystalline VO_2 nanobelts can be prepared into stable colloidal solutions, or assembled into paper forms by tuning process parameters. The morphology of the samples can be adjusted by varying the parameters of the solution. The electrical transport through single nanobelts was investigated and the magnetic measurement showed VO_2(B) was a paramagnetic material. This hydrothermal method should be applicable for large-scale production of low-dimensional nanostructured vanadium dioxides.

Experimental Section

The vanadium dioxide nanobelts were synthesized under hydrothermal conditions. All chemicals were purchased from the Beijing Chemical Reagents Company and were used without further purification. In a typical synthesis, ammonium metavanadate (0.234 g) was dissolved in deionized water to form a light yellow clear solution. Formic acid was added dropwise to the ammonium metavanadate solution (0.1M; 20 mL) until the final pH of the solution was about 2–3 under stirring. A clear orange solution was formed and the resultant solution was then transferred into a Teflon-lined autoclave with a stainless-steel shell. The autoclave was kept at 180°C for two days and then allowed to cool to room temperature. The final product was washed with deionized water and pure alcohol

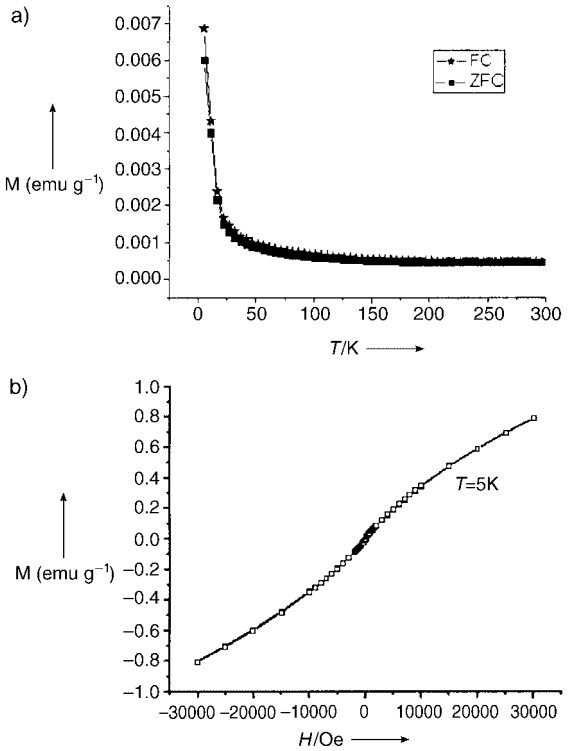

Figure 5. a) ZFC and FC curves of vanadium dioxide nanobelts measured with the field of 100 Oe. b) Magnetization of vanadium dioxide nanobelts plotted as a function of the applied field measured at 5 K.

several times to remove any other possible residues and then dried at 60 °C under vacuum for 6–8 h.

Powder X-ray diffraction (XRD) experiments on the products were conducted on a Bruker D-8 Avance X-ray diffractometer with $Cu_{K\alpha}$ radiation ($\lambda = 1.5418$ Å). The morphologies and structures of the vanadium dioxide nanobelts were observed at 200 kV by using a LEO-1530 field-emission scanning electron microscope (FE-SEM), a Hitachi H-800 transmission electron microscope (TEM), and a JEOL JEM-2010F high-resolution transmission electron microscope (HRTEM). Electron diffraction (ED) patterns were used to determine the growth orientation of the as-prepared 1D product.

Received: March 24, 2004

Keywords: electrical transport · hydrothermal synthesis · magnetic properties · nanostructures · vanadium

[1] H. J. Dai, E. W. Wong, C. M. Lieber, *Science* **1996**, *272*, 523.
[2] D. Bozovic, M. Bockrath, J. H. Hafner, C. M. Lieber, H. Park, M. Tinkham, *Appl. Phys. Lett.* **2001**, *78*, 3693.
[3] H. J. Dai, *Acc. Chem. Res.* **2002**, *35*, 1035.
[4] H. Kind, H. Q. Yan, B. Messer, M. Law, P. D. Yang, *Adv. Mater.* **2002**, *14*, 158.
[5] J. Zhou, N. S. Xu, S. Z. Deng, J. Chen, J. C. She, Z. L. Wang, *Adv. Mater.* **2003**, *15*, 1835.
[6] X. F. Duan, Y. Huang, R. Agarwal, C. M. Lieber, *Nature* **2003**, *421*, 241.
[7] J. A. Zapien, Y. Jiang, X. M. Meng, W. Chen, F. C. K. Au, Y. Lifshitz, S. T. Lee, *Appl. Phys. Lett.* **2004**, *84*, 1189.
[8] J. J. Urban, J. E. Spanier, O. Y. Lian, W. S. Yun, H. Park, *Adv. Mater.* **2003**, *15*, 423.
[9] J. Q. Hu, Y. Bando, Z. W. Liu, J. H. Zhan, D. Golberg, T. Sekiguchi, *Angew. Chem.* **2004**, *116*, 65; *Angew. Chem. Int. Ed.* **2004**, *43*, 63.
[10] D. Mann, A. Javey, J. Kong, Q. Wang, H. J. Dai, *Nano Lett.* **2003**, *3*, 1541.
[11] C. N. R. Rao, A. K. Cheetham, *J. Mater. Chem.* **2001**, *11*, 2887.
[12] C. N. R. Rao, G. U. Kulkarni, P. J. Thomas, P. P. Edwards, *Chem. Eur. J.* **2002**, *8*, 29.
[13] Y. N. Xia, P. D. Yang, Y. G. Sun, Y. Y. Wu, B. Mayers, B. Gates, Y. D. Yin, F. Kim, Y. Q. Yan, *Adv. Mater.* **2003**, *15*, 353.
[14] G. R. Patzke, F. Krumeich, R. Nesper, *Angew. Chem.* **2002**, *114*, 2554; *Angew. Chem. Int. Ed.* **2002**, *41*, 2446.
[15] C. N. R. Rao, M. Nath, *Dalton Trans.* **2003**, 1.
[16] C. N. R. Rao, F. L. Deepak, G. Gundiah, A. Govindaraj, *Prog. Solid State Chem.* **2003**, *31*, 5.
[17] W. Li, J. R. Dahn, D. S. Wainwright, *Science* **1994**, *264*, 1115.
[18] C. Tsang, A. Manthiram, *J. Electrochem. Soc.* **1997**, *144*, 520.
[19] Z. Gui, R. Fan, W. Q. Mo, X. H. Chen, L. Yang, S. Y. Zhang, Y. Hu, Z. Z. Wang, W. C. Fan, *Chem. Mater.* **2002**, *14*, 5053.
[20] W. U. Huynh, J. J. Dittmer, A. P. Alivisatos, *Science* **2002**, *295*, 2425.
[21] F. Theobald, R. Cabala, J. Bernard, *J. Solid State Chem.* **1976**, *17*, 431.
[22] A. M. Kannan, A. Manthiram, *Solid State Ionics* **2003**, *159*, 265.
[23] C. Leroux, G. Nihoul, G. Van Tendeloo, *Phys. Rev. B* **1998**, *57*, 5111.

